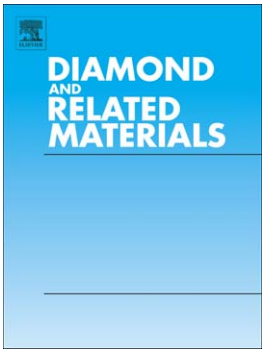

Electrical and Raman-imaging characterization of laser-made electrodes for 3D diamond detectors

S. Lagomarsino, M. Bellini, C. Corsi, S. Fanetti, F. Gorelli, I. Liontos, G. Parrini, M. Santoro, S. Sciortino

PII: S0925-9635(14)00004-1
DOI: doi: 10.1016/j.diamond.2014.01.002
Reference: DIAMAT 6210

To appear in: *Diamond & Related Materials*

Received date: 7 October 2013
Revised date: 19 December 2013
Accepted date: 4 January 2014

Please cite this article as: S. Lagomarsino, M. Bellini, C. Corsi, S. Fanetti, F. Gorelli, I. Liontos, G. Parrini, M. Santoro, S. Sciortino, Electrical and Raman-imaging characterization of laser-made electrodes for 3D diamond detectors, *Diamond & Related Materials* (2014), doi: 10.1016/j.diamond.2014.01.002

Electrical and Raman-imaging characterization of laser-made electrodes for 3D diamond detectors

S. Lagomarsino[1,2,*], M. Bellini[3,4], C. Corsi[3], S. Fanetti[3], F. Gorelli[3,4], I. Liontos[3,5], G. Parrini[1,2], M. Santoro[3,4] and S. Sciortino[1,2]

[1] National Institute of Nuclear Physics (INFN), Via B. Rossi 1-3, 50019 Sesto Fiorentino (FI), Italy.

[2] Department of Physics and Astronomy, University of Florence, Via G. Sansone 1, 50019 Sesto Fiorentino (FI), Italy

[3] European Laboratory for Non-Linear Spectroscopy, Via Nello Carrara 1, 50019 Sesto Fiorentino (FI), Italy

[4] Istituto Nazionale di Ottica (INO-CNR), Largo Enrico Fermi 6, 50125 Firenze (FI) Italy

[5] Center for Plasma Physics and Lasers (CPPL), 1 E. Daskalaki Str., 74100 Rethymno (Crete), Greece

Abstract

Pulsed laser writing of graphitic electrodes in diamond is a promising technique for innovative particle detectors. Although of great relevance in 3D fabrication, the processes involved in sub-bandgap bulk irradiation are still not well understood. In this work, Raman imaging is exploited to correlate resistivity and graphitic content in 5÷10 μm-thick electrodes, obtained both in the domains of femtoseconds and of nanoseconds of pulse duration. A wide interval of resistivities (60-900 mΩcm), according to the irradiation technique employed, are correlated with an sp^2 content of the modified material ranging over a factor 2.5. The stress distribution (maximum of about 10 GPa) and the presence of nano-structured sp^3 material around the graphitic columns have also been studied by Raman spectroscopy, and a rationale for the conductive behaviour of the material is presented in terms of the thermodynamics of the process.

*corresponding author: Stefano Lagomarsino, lagomarsino@fi.infn.it

1. Introduction

Diamond detectors have long been envisaged as a promising solution for the challenges of radiation-harsh environments[1], and are now assuming an important role in R&D activities for the upgrade of the innermost tracking layers at the Large Hadron Collider (LHC) at CERN[2,3].

Qualities which make diamond a good candidate are the high saturation velocity of the charge carriers (double as high as for silicon), the low dielectric constant (5.6 vs 11.9 for silicon), the extremely low leakage currents (at most 10^{-3} times those of silicon at the same bias voltages and temperatures), the high operative temperatures (tested[4] up to 80 °C) and, most importantly, a very high knock-on energy (about 50 eV, vs. 15 eV for silicon[5]), which contributes to an extremely favorable tolerance to radiation damage.

The advantages of diamond on silicon become even more effective in the 3D concept, developed in the last decades for silicon detectors[6,7]. In this architecture the charge collection is accomplished by narrow columnar electrodes which, being normal to the sensor larger surfaces, are nearly parallel to the path of the particles crossing the sensor itself. In this way both the response speed and the radiation tolerance take a further advance due to the shortening of the carrier paths, which depends on the distance between electrodes, which is much lower than the material thickness.

Although micro-fabrication of buried structures in diamond could also be possible with techniques employing MeV ion irradiation[8, 9], pulsed laser graphitization is a technique which offers a much easier way to fabricate conductive channels orthogonal to the diamond surface[10]. This is, at present, the technique used for fabrication of 3D electrodes[11,12,13]. Nevertheless, in spite of the progresses in their implementation, graphitic structures in the diamond bulk exhibit a resistivity[14] two order of magnitude higher than that reported for amorphous graphite, and the production of mechanical cracks in the diamond structure is still an issue. Moreover, although Raman analysis evidenced the presence of a

graphitic phase in the buried conductive channels[14], there is a lack of quantitative studies correlating the Raman signature with the peculiar conductive behavior of this material.

In this work, we fabricated conductive structures both on the surface and in the bulk of diamond by means of pulsed laser irradiation with pulse widths in the nanosecond and the femtosecond domains, and we performed their quantitative characterization by means of micro-Raman imaging, with a resolution of ~2 μm. We extracted information about the local phase composition of the obtained structures in term of sp^2 and sp^3-bonded carbon concentrations, evidencing a strong correlation between their conductivity and their graphitic content. Information about the local stress conditions were also obtained, from which a rationale for the different phase composition of structures fabricated under different local conditions is given, involving the thermodynamics of the process.

2. Material and methods

We used polycrystalline and monocrystalline detector-grade diamond samples by Element Six. This kind of material is usually defined[15] as a type IIa diamond exhibiting a minimum charge collection distance of about 200 μm. The pulsed laser sources employed were:

a) a Nd:YAG Q-switched source with an 8 ns pulse width, 1064 nm wavelength, pulse energies in the range 10-60 μJ and repetition rates from 1 to 10 kHz.

b) a Ti:sapphire femtosecond laser source of 30 fs pulse width, 800 nm wavelength, pulse energies between 3 and 18 μJ and repetition rate of 1 kHz.

Both beams have been focused either on the diamond surface or in the diamond bulk with microscope objectives optimized for the wavelengths of interest. The waist in the two cases had about the same diameter, in the range 8-10 μm. The same objectives were also used to acquire optical micrographs of the sample during the irradiation, with the aid of a suitably arranged microscope system (see fig. 1).

The sample position was controlled by a three-axes displacement stage driven by computerized step

motors with micrometric resolution.

The experimental setup has been arranged in a way that it is possible to switch from a laser source to the other without moving the sample and allowing, if necessary, an easy integration of the two techniques in processing the same device.

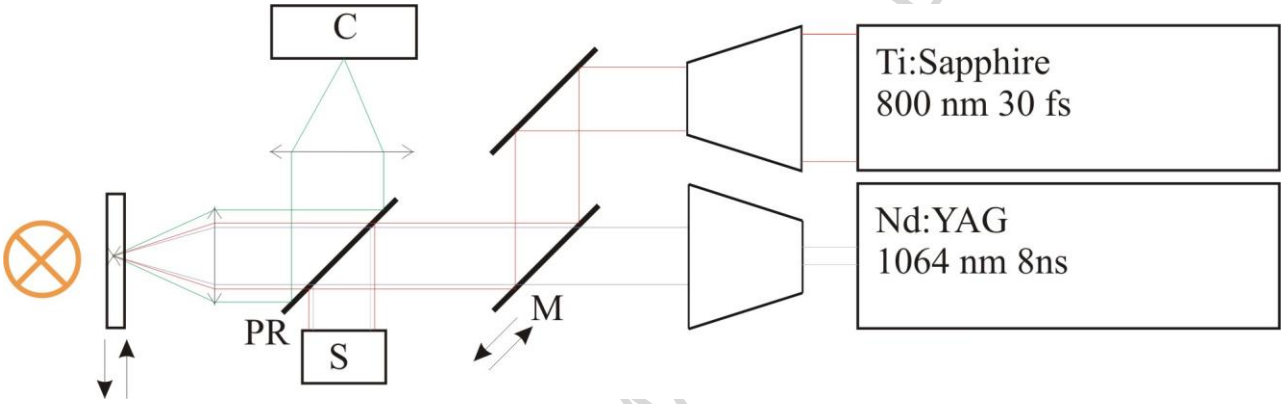

Figure 1. Experimental set-up used to fabricate graphitic structures in diamond. The sample is moved with respect to the laser beam by an *xyz* interfaced system. Mirror M allows to switch from one source to another. The images of the sample (illuminated in transparency) and the laser spot is collected by the camera C. The power at target is monitored by the power-meter S.

The graphitic structures we implemented are: A) Superficial conductive tracks obtained by keeping the front surface of diamond in the focal plane of the objective and translating it at constant velocity (*xy*-directions). B) Buried conductive wires obtained by focusing the laser beam on the back diamond surface and moving the focus at constant velocity perpendicularly to the surface, across the bulk for 100-500 μm (z-direction).

Figure 2A shows a 3D structure made of staggered wires, fabricated with the fs-laser source, connected with two interdigitated superficial graphitic combs engraved with the nanosecond laser irradiation. We fabricated structures of up to 310 columns in 2-dimensional arrays covering areas 1.5×1.5 mm^2. In Figure 2B and 2C two buried columns created by the ns and the fs-laser source are shown, as seen across a lateral polished surface at about 40 μm from each column.

The electrical transport properties of the tracks fabricated on the surface and across the diamond have been measured with standard current-voltage measurements, resulting in a good ohmic behavior. Their geometric shape was determined by optical inspection, in a way to calculate the electrical resistivity of the graphitic phases created by laser irradiation.

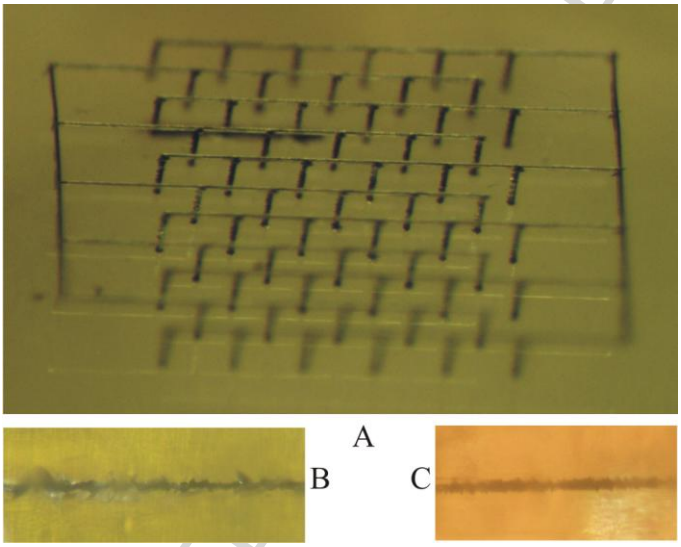

Figure 2. A: 1x1 mm^2 3D structure consisting of 36 + 25 = 61 staggered vertical wires 500 μm long, connected to interdigitated graphitic combs on a same surface of diamond. The distance between the comb teeth is 100 μm. The wires appears to be shorter than they are because of the refraction.
B: Image of a wire fabricated with the nanosecond laser source
C: image of a wire fabricated with the femtosecond laser source.
The image of the wire in C appears to be sharper because of the refraction on the cracks created in B by the nanosecond source.

Since the conductive behavior of the material appears to be strongly dependent on the conditions of irradiation and on the laser source employed (see section Results and Discussion), a micro-Raman characterization of the graphitic phases has been performed, in order to correlate morphology and electrical conductivity with the phase composition of the artifact. The experimental apparatus, which is described in detail elsewhere[16], has a lateral spatial resolution of about 3 μm, and a field depth of the same order. The wavelengths employed were mainly 647 nm and 752 nm from a Kr laser lines. The superficial tracks, as well as the emerging ends of the buried columns, were analyzed by focusing the beam on the surface of the sample. The spectra of columnar buried structures were observed across the

lateral polished surface of the diamond slice, placed at the fixed distance of 40 μm from the graphitic column, in a way that the analysis of the spectra of different columns allows a quantitative comparison of the phase content. An *xy* motorized displacement system was exploited, in order to obtain 2-dimensional Raman images of the field of view.

3. Results and Discussion

Superficial and buried conductive channels have different morphological, electrical and structural characteristics, according to the laser source employed.

3.1 *Superficial tracks*

Only the ns-pulsed laser source appears to be useful in fabrication of superficial conductive track, because the fs-laser source causes ablation of diamond, and leaves only a very thin layer of modified material. On the contrary, the ns-laser source creates deep (up to 50 μm) and narrow (~10 μm) channels uniformly filled with an opaque material, which results ablated only for a depth from 3 to 7 μm.

The depth of the channels increases with the number of laser pulses impinging on a same point, reaching about 50 μm at about 700 pulses-per-point (see fig. 3). On the contrary, it is quite independent on the pulse energy (at least up to 50 μJ-per-pulse), provided that the energy lies above a threshold of about 6 μJ-per-pulse. This is the threshold found if the irradiation starts from a zone where the material is already graphitized, while if graphitization has to start from undamaged diamond the threshold is placed at about 37 μJ-per-pulse.

The resistivity of the material, as measured on different tracks fabricated with different energy-per-pulse and number of pulses-per-point, is quite dispersed (8 ± 4 mΩcm, see tab. I) around a value which is not so far from those reported for amorphous graphite ($0.4 \div 5$ mΩcm), with no clear dependence on the process parameters.

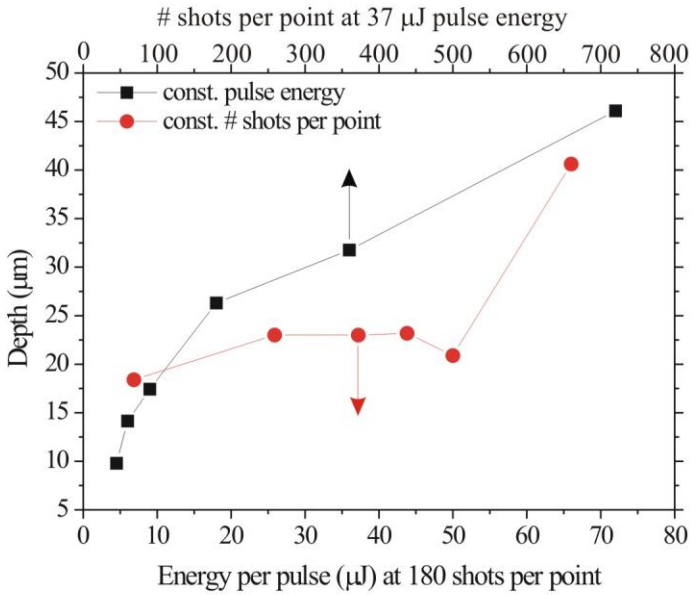

Figure 3. Red points: depth of the superficial tracks made with the ns-pulsed laser source as a function of energy per pulse (at constant number of shots per point) . Black points: depth of the tracks as a function of the number of shots per point (at constant energy).

Material	Resistivity (mΩcm)
Superficial tracks (ns laser source)	8±4
Buried wires (ns laser source)	60±20
Buried wires (fs laser source)	900±300

Table 1. Comparison between the resistivity of different kind of graphitic materials, created in different location (superficial or buried), and with different laser sources.

Raman characterization confirms the suggestion, resulting from the measurement of the resistivity, that the modified material consists in a phase of disordered sp^2 carbon.

We examined the spectra of the material emerging at the free surface of diamond, and in all cases we found invariantly a feature with two wide peaks centered at 1325 cm^{-1} and 1580 cm^{-1} (see Fig.4).

While the 1580 cm^{-1} peak is easily identified as the G-peak of amorphous graphite[17] the assignment of

the peak at 1325 cm^{-1} was more sophisticated. It could be due to the reported D-peak of disordered graphite[17] but its position close to the diamond Raman line could make it possible to attribute it to nanocrystalline diamond[18,19]. Since the D-peak of graphite is known to have a dispersive behavior as a function of the exciting radiation frequency, we performed Raman measurements of the position of the peak at different wavelengths (514, 532, 647 and 752 nm) in order to discriminate the two possibilities. The dispersive behavior observed for this feature for excitation lines from green to red (see the inset of figure 2) is consistent with the existing literature about the graphite D-peak, allowing to conclude that the superficial modified material consists in disordered graphite.

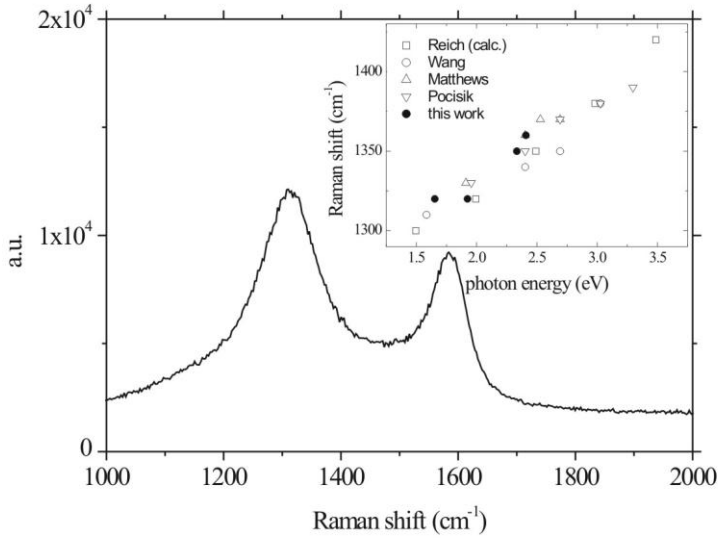

Figure 4. Raman spectrum of a typical superficial graphitization. In the inset, the dispersive behavior of the D-peak, compared with those reported in literature for the corresponding peak of disordered graphite (references in Reich *et al.*[17]).

3.1 *Buried columns*

Both the sources we employed are capable to write buried conductive wires perpendicular to the beam entrance surface of diamond, but with different geometrical and physical characteristics. The cross-sectional area of both types of structure depends on the pulse energy, being roughly proportional to the

difference between the pulse energy and a threshold value which is about 2 μJ for the fs-pulsed laser source and 9 μJ for the ns-one (see fig. 5). In the case of ns-pulsed laser, in order to grow a buried column with such a low value of the energy-per-pulse, it is necessary to initiate it on an already graphitized zone on the back side of the diamond sample.

The morphological characteristics of the two kinds of columns are quite different: ns-laser made structures are quite irregular in cross-section and exhibit cracks which are more and more evident as the value of the energy-per-pulse increases (see fig. 2B and 2C). On the contrary, fs-laser made columns are more regular in section and show traces of ruptures only for very high values of the energy-per-pulse employed.

The two types of wires also exhibit a very different electrical behavior. The mean resistivity obtained for the ns-source wires was about 60 mΩcm, while that for the fs-source wires was an order of magnitude greater (about 900 mΩcm, see Tab. I) in agreement with Kononenko *et al*.[14]

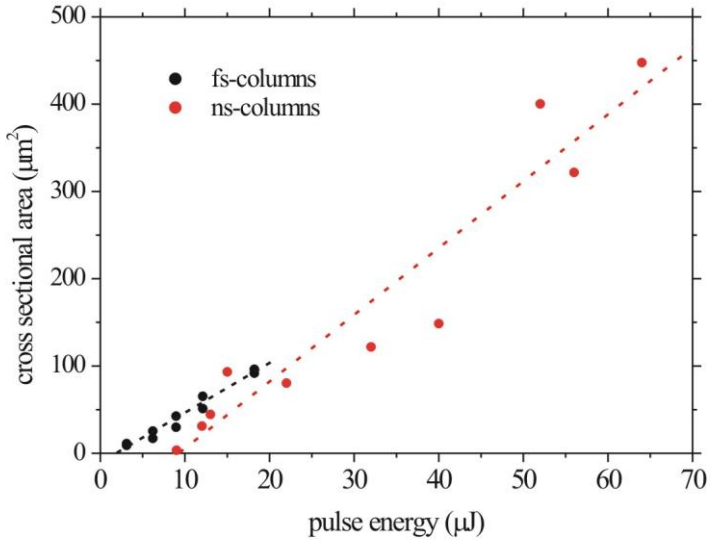

Figure 5: The cross-sectional area of both types of columns (made with the ns and fs laser respectively) are roughly proportional to the difference between the pulse energy and a threshold value.

The Raman analysis of the two kind of structures explains the difference in their electrical behavior.

While the spectra of the emerging part each column show substantially no difference with that shown in figure 3, those of the buried part are well represented by fig. 6

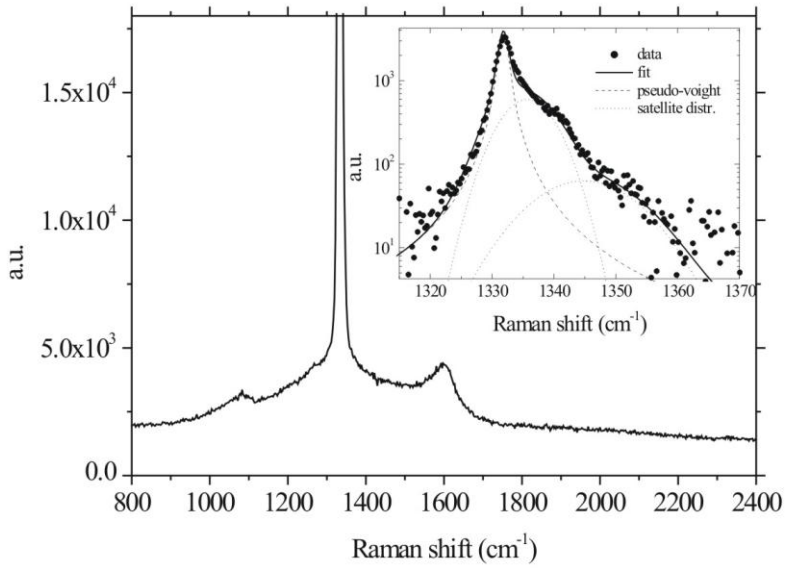

Figure 6. Raman spectrum of a buried graphitic wire fabricated with the nanosecond laser source. In the inset: a detail in the 1310-1370 range, showing the distortion of the diamond peak due to the mechanical stress.

The 1332 cm^{-1} line of diamond is superimposed to the D peak, due to the 40 μm-thick layer of diamond in front of each column, and a distinct G peak at 1580 cm^{-1} is detectable along the axis of our buried structures, confirming the presence of graphite inside the fabricated buried patterns. Moreover, a feature at 1090 cm^{-1} is seen, in the wires fabricated with the ns-pulsed laser source, around the graphitic structures within a distance of a few micrometers, while for the wires created with the femtosecond laser its presence is assessed with a much lower intensity and only sporadically. This peak is attributed to nano-crystalline diamond[20], or to Z-carbon[21], an sp^3 phase which is stable at pressures exceeding about 9.8 GPa. The local pressure, on the other hand, can be studied considering the stress-induced deformation of the diamond line at 1332 cm^{-1} (see the inset of fig 5), acquiring information about the physical state of the graphitic phase itself.

To extract quantitative information about the content in graphite of buried structures, we compared the areas A_G under the G peak with those under the peak of diamond (A_{Dia}) at the same depth inside the diamond bulk but quite far from the graphitic column, in order to use A_{Dia} as a monitor of the laser beam intensity. The index $r = \frac{A_G}{A_{Dia}}$ is taken as an indication of the quantity of graphite.

The images of figure 7 (top of the figure) shows 20×20 μm^2 2-dimensional profiles of the *r* index for two different graphitic wires, fabricated with the nanosecond and the femtosecond pulsed source respectively.

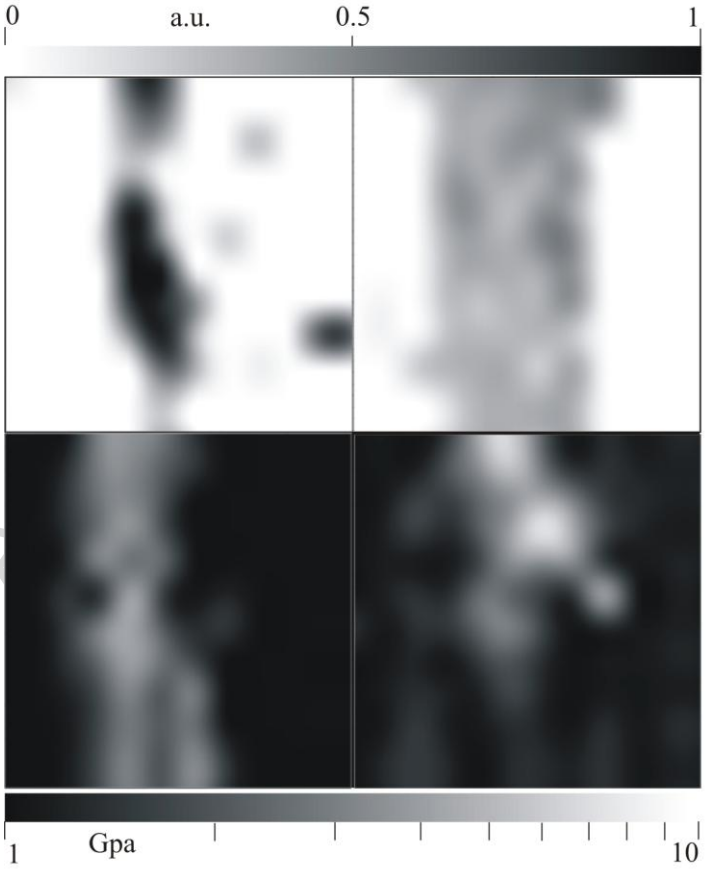

Figure 7. Top of the figure: maps of the G-peak intensity (*r* index in the text) for wires created with the nanosecond (left) and the femtosecond (right) laser source, corresponding to regions of 20×20 μm^2. Bottom of the figure: maps of the P_{max} index corresponding to the same regions (left for the nanosecond, right for the femtosecond wire).

We found that the maximum *r* index measured in the patterns created with the femtosecond and the

nanosecond laser sources are in the ratio 1 : 2.5. Thus, it is proved that the resistivity of differently fabricated structures is related to the different content in graphite of the material. The picture suggested is that of a mixture of two phases in which conduction takes place by percolation between graphite micro or nano-crystals dispersed in an sp^3 matrix.

As a matter of fact, the presence of an sp^3 phase is well assessed at least in the buried structures created with the nanosecond laser source.

In figure 8 (top of the figure) 2-dimensional profiles of the intensity of the 1090 cm^{-1} line attributed to diamond nanocrystals or to Z-carbon is shown for two different columns, one of which corresponding to the top-left map of figure 7. It is apparent the correlation with the graphite-map profile, suggesting the presence of a defective layer around the graphitic path.

Now we can give an account of the Raman measurement of the pressure distribution around the buried graphitized columns, from which a rationale for the different composition of the superficial and the buried patterns can be inferred.

We found that the diamond peak is strongly distorted in the region of the buried structures (see the inset of Fig. 5). Its shape can be described by a superposition of a standard pseudo-Voigt profile centered at 1332 cm^{-1} with a FWHM of about 1.8 cm^{-1} with a wide feature whose best fit is accomplished by one, two or (occasionally) more gaussian profiles, mainly but not exclusively centered at higher wavenumbers.

We interpreted the 1332 cm^{-1} peak as due to the undistorted profile of the diamond layer at great distance from the graphitic track, while the satellite profile, whose width is generally greater than that of the diamond line, is interpreted as an inhomogeneous distortion produced by the highly stressed material around and inside the structures under study. The cubic structure of diamond allows the reasonable assumption that the shape of the satellite profile is almost uniquely related to the uniaxial pressure-tension distribution along the line of sight, irrespective of the crystal orientation.

Thus, we assumed as an index of the maximum compressive stress P_{max} along the line of sight the

Raman shift displacement $\Delta\nu$ corresponding to the 84th percentile of the satellite distribution (in analogy with the cumulate of a standard distribution at the average plus the standard deviation) divided by the constant 2.44 cm^{-1}GPa^{-1}, as suggested by Akamaha *et al.*[22] for pressures below some tens of GPa.

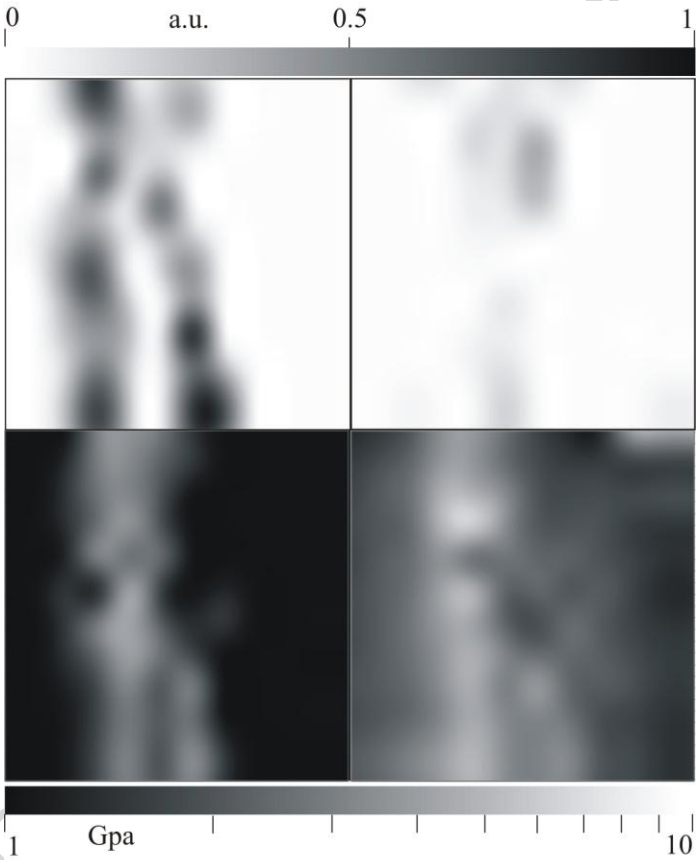

Figure 8. Top of the figure: maps of the intensity of the peak at 1090 cm^{-1} for two different wires created with the nanosecond laser source, both with a pulse energy of 9 μJ and a sample translating velocity of 250 μm/s, but with pulse rates respectively of 5000 Hz (left) and 500 Hz (right). Both images refer to regions of 20×20 μm^2, the firs one is the same of figure 4 (left). Bottom of the figure: maps of the P_{max} index corresponding to the same regions.

Fig. 7 and 8 (bottom of the figures) show two-dimensional maps of P_{max} spatially coinciding with those shown in the top of the same figures. It is apparent that the regions occupied by the graphitic phase and by the sp^3 nanostructured phase are related to a compressive stress in the diamond around them which can be as high as 10 GPa, not so far from the maximum pressure for which graphite is stable at the thermodynamic equilibrium, that is the graphite-diamond-liquid triple point pressure, about 13 GPa[23].

This explains the reduced graphitic content and the high values of resistivity of the buried material. The very high elastic constants of diamond and graphite and the low density of graphite with respect to diamond would determine, in the case of a complete transformation of diamond in graphite, very high pressure of the buried graphitic phases, which can be estimated in about 60 GPa*. But graphite is stable at the thermodynamic equilibrium only below about 13 GPa. Consequently, only a high density mixed phase can crystallize, in a way that the local pressure never exceeds, after the phase formation, those permitted by the thermodynamics. A high density phase can be obtained only in a material relatively poor of sp^2 bonds, determining an intrinsic higher resistivity of the buried graphitic electrodes with respect to the surface ones.

This picture is confirmed by Raman analysis of the emerging part of the buried columns, where the pressure is supposed to be the atmospheric one. This spectra, as just said, are the same of those obtained by the superficial tracks, and completely compatible with those of amorphous graphite.

3. Conclusions

A correlation between Raman signatures and resistivity values of graphitic wires has been assessed. The channels fabricated with the ns laser exhibit a lower resistivity due to the higher abundance of the sp^2 phase. On the other hand, a defective layer of nanocrystalline sp^3 material has been evidenced around the ns-wires.

In spite of the relatively high resistances of the buried wires made with the fs-laser source, and of the presence of a defective layer in those made with the ns-one, measurements of charge collection efficiency in diamond particle sensors formed by arrays of buried graphitic columns, attest their

* An approximate calculation based on the assumption that the cubic diamond lattice behaves like an isotropic material, as well as amorphous graphite, gives, for a cylindrical column, a pressure given by $P = \frac{\left(C_{11}^D - C_{44}^D\right)\left(C_{11}^G + C_{44}^G\right)}{C_{11}^D - C_{44}^D + C_{11}^G + C_{44}^G}\left(\sqrt{\frac{\delta_D}{\delta_G}} - 1\right)$, where $\delta_{D,G}$ is the density of diamond or graphite at standard pressure and $C_{kk}^{D,G}$ are the elastic constants of diamond and amorphous graphite[24].

suitability as electrodes and their full compatibility with a standard readout electronics[24]. Nonetheless, the employment of the fs-columns in a pixel detector, where each readout line is connected with a single column, would determine a high level of Johnson noise, while defective layers around the ns-columns could result in a signal degradation. For this reason, investigation on the physical properties of this material is necessary, in order to find the best compromise in the process parameters and in the geometric tailoring of 3D-electrodes which, potentially, can be a breakthrough in radiation-hard detectors for high energy physics.

Acknowledgements

We are grateful to Andrea Giugni and Gobind Das, (IIT Genova – Italy) for performing some of the Raman measurement of Figure 2. We are also grateful to Mauro Pucci (INO-Florence - Italy) for his work in optical and mechanical processing of diamond samples and to Mirko Brianzi (INFN-Florence - Italy) for his help in the electrical measurements. We acknowledge the support from the European Union (LENS Contract FP7 G.A.No. 228334 LASERLABEUROPE), the Ente Cassa di Risparmio di Firenze, and the Deep Carbon Observatory initiative (Grant N. 2011-10-01 from the Alfred P. Sloan Foundation for the project entitled 'Physics and Chemistry of Deep Carbon Bearing Fluids and Mineral').This work was accomplished in the framework of the INFN experiment CHIPSODIA.

Diamond and Related Materials

PRIME NOVELTY Statement

Please provide a **Prime Novelty Statement** for your manuscript below (one or two sentences). This statement should provide information as to what is new and novel in the manuscript, and is provided to referees for consideration when reviewing manuscripts.

We have performed for the first time a Raman imaging characterization of buried graphitic electrodes in Diamond, obtaining space-resolved information about phase composition and state of stress of laser-made graphitic structures, fabricated with ns- and fs-pulsed laser sources.

We have correlated electrical resistivity and graphitic content of laser-modified diamond material.

We have compared graphitic electrodes made by laser at different pulse widths, in the range of nanosecond and femtoseconds and discovered the presence of an sp^3 disordered phase around the electrodes made with the ns source, exhibiting a Raman peak at 1090 cm^{-1}.

Highlights

Fabrication of superficial and buried graphitic structures in diamond by means of ns- and fs-pulsed laser radiation.
Quantitative two-dimensional maps of the phase composition and of the stress conditions of the artifacts were obtained by micro-Raman imaging.
A correlation between electrical conductivity and graphitic content was assessed.
A rationale for the different composition of phases obtained in different condition has been found, involving the thermodynamics of the process.

References

[1] R. Tapper, Diamond detectors in particle physics, Rep. Prog. Phys. 63 (2000) 1273–1316

[2] D. Asnar, et al., The RD42 Collaboration, Diamond pixel modules, Nucl. Instr. & Meth A 636 (2011) S125–S129

3 L.Uplegger, et al., Test-beam studies of diamond sensors for SLHC, Nucl. Instr. & Meth A (2012), http://dx.doi.org/10.1016/j.nima.2012.10.011

[4] R. D'alessandro, F. Hartjes, S. Lagomarsino, S. Sciortino, Influence of temperature on the response of high-quality polycrystalline diamond detectors, Nuclear Instruments and Methods in Physics Research A 570 (2007) 303–307.

[5] W. Wu, S. Fahy, Molecular-dynamics study of single-atom radiation damage in diamond, Phys. Rev. B 49, 3030–3035 (1994)

[6] J Segal S. I. Parker C. J. Kenney. A proposed new architecture for solid-state radiation detectors. In: Nucl. Instr. and Meth. A 395 pp 328-343 (1997)

[7] C. D. Via, E. Bolle, K. Einseweiler, M. Garcia-Sciveres, J. Hasi, C. Kenney, V. Linhart, S. Parker, S. Pospisil, O. Rohne, T. Slavicek, S. Watts, N. Wermes. 3d active edge silicon sensors with different electrode configurations: Radiation hardness and noise performance, Nuclear instruments and methods in physical research A. 604 (2009) 505–511.

[8] P. Olivero, J. Forneris, M. Jakšic, Z. Pastuovic, F. Picollo, N. Skukan, E. Vittone, Focused ion beam fabrication and IBIC characterization of a diamond detector with buried electrodes, Nucl. Instr. & Meth A B 269 (2011) 2340–2344

[9] S. Lagomarsino, P. Olivero, F. Bosia, M. Vannoni, S. Calusi, L. Giuntini, M. Massi. Evidence of light guiding in Ion-implanted Diamond. Phys. Rev. Lett. 105, 233903 (2010)

[10] T.V. Kononenko, M.S. Komlenok, V.P. Pashinin, S.M. Pimenov, V.I. Konov, M. Neff, V. Romano, W. Lüthy, Femtosecond laser microstructuring in the bulk of diamond, Diamond and Relat. Mater. 18 (2009) 196–199

[11] A. Oh, B. Caylar, M. Pomorsky, T. Wengler. A novel detector with graphitic electrodes in CVD diamond. Diamond & Related Materials 38 (2013) 9–13.

[12] T.V. Kononenko, A.A. Khomich, V.I. Konov. Peculiarities of laser-induced material transformation inside diamond bulk. Diamond & Related Materials 37 (2013) 50–54.

[13] S. Lagomarsino, M. Bellini, C. Corsi, F. Gorelli, G. Parrini, M. Santoro and S. Sciortino. 3D Diamond detectors: charge collection efficiency of graphitic electrodes. In press for Applied Physics Letters.

[14] T.V. Kononenko, V. Konov, S. Pimenov, N. Rossukanyi, A. Rukovishnikov, V. Romano, Three-dimensional laser writing in diamond bulk, Diamond and Related Materials 20 (2011) 264–268.

[15] H. Kagan and W. Trischuk. Radiation Sensors for High Energy Physics Experiments, In "CVD Diamond for Electronic Devices and Sensors", John Wiley and Sons Ltd (2009)

[16] M. Ceppatelli, F.A. Gorelli, J. Haines, M. Santoro and R. Bini. Probing high pressure reactions in heterogeneous materials by Raman spectroscopy, in press in Z. Cristallogr. (2013) DOI 10.1515/zkri-2014-1627

[17] Stephanie Reich and Christian Thomsen, Raman spectroscopy of graphite, Phil. Trans. R. Soc. Lond.,15 November 2004 vol. 362 , 2271-2288

[18] M. Yoshikawa, Y. Mori, H. Obata, M. Maegawa, G. Katagiri, H. Ishida, and A. Ishitani. Raman scattering from nanometer-sized diamond. Appl. Phys. Lett. 67 (1995) 694-696

[19] S. Osswald, V.N. Mochalin, M Havel, G. Yushin, and Y. Gogotsi. Phonon confinement effects in the Raman spectrum of nanodiamond. Phys. Rev. B 80 (2009) 075419

[20] S. Prawer , K.W. Nugent, D.N. Jamieson, J.O. Orwa, L.A. Bursill, J.L. Peng. The Raman spectrum of nanocrystalline diamond. Chem. Phys. Lett. 332 (2000) 93-97.

[21] Maximilian Amsler, Jose´ A. Flores-Livas, Lauri Lehtovaara, Felix Balima, S. Alireza Ghasemi, Denis Machon, Ste´phane Pailhe`s, Alexander Willand, Damien Caliste, Silvana Botti, Alfonso San Miguel, Stefan Goedecker, and Miguel A. L. Marques. Crystal Structure of Cold Compressed Graphite. Phys. Rev. Lett. 108 (2012) 065501-4

[22] Y. Akahama Y and H. Kawamura, J. Appl. Phys. Pressure calibration of diamond anvil Raman gauge to 310 GPa, 100 (2006) 043516

[23] Laurence E. Fried and W. Michael Howard. Explicit Gibbs free energy equation of state applied to the carbon phase diagram. Phys. Rev. B 61 (2000) 8734-8743

[24] S. Lagomarsino, M. Bellini, C. Corsi, F. Gorelli, G. Parrini1, M. Santoro and S. Sciortino. Three-dimensional diamond detectors: Charge collection efficiency of graphitic electrodes, Appl. Phys. Lett. **103**, 233507 (2013).

[24] P.C.Kelires. Physical Review Letters, **73** (1994) 2460-3

Figure Captions

Figure 1. Experimental set-up used to fabricate graphitic structures in diamond. The sample is moved with respect to the laser beam by an *xyz* interfaced system. Mirror M allows to switch from one source to another. The images of the sample (illuminated in transparency) and the laser spot is collected by the camera C. The power at target is monitored by the power-meter S.

Figure 2. A: 1x1 mm^2 3D structure consisting of 36 + 25 = 61 staggered vertical wires 500 μm long, connected to interdigitated graphitic combs on a same surface of diamond. The distance between the comb teeth is 100 μm. The wires appears to be shorter than they are because of the refraction.
B: Image of a wire fabricated with the nanosecond laser source
C: image of a wire fabricated with the femtosecond laser source.
The image of the wire in C appears to be sharper because of the refraction on the cracks created in B by the nanosecond source.

Figure 3. Red points: depth of the superficial tracks made with the ns-pulsed laser source as a function of energy per pulse (at constant number of shots per point) . Black points: depth of the tracks as a function of the number of shots per point (at constant energy).

Figure 4. Raman spectrum of a typical superficial graphitization. In the inset, the dispersive behavior of the D-peak, compared with those reported in literature for the corresponding peak of disordered graphite (references in Reich *et al*.[17]).

Figure 5: The cross-sectional area of both types of columns (made with the ns and fs laser respectively) are roughly proportional to the difference between the pulse energy and a threshold value.

Figure 6. Raman spectrum of a buried graphitic wire fabricated with the nanosecond laser source. In the inset: a detail in the 1310-1370 range, showing the distortion of the diamond peak due to the mechanical stress.

Figure 7. Top of the figure: maps of the G-peak intensity (*r* index in the text) for wires created with the nanosecond (left) and the femtosecond (right) laser source, corresponding to regions of 20×20 μm^2. Bottom of the figure: maps of the P_{max} index corresponding to the same regions (left for the nanosecond, right for the femtosecond wire).

Figure 8. Top of the figure: maps of the intensity of the peak at 1090 cm^{-1} for two different wires created with the nanosecond laser source, both with a pulse energy of 9 μJ and a sample translating velocity of 250 μm/s, but with pulse rates respectively of 5000 Hz (left) and 500 Hz (right). Both images refer to regions of 20×20 μm^2, the firs one is the same of figure 4 (left). Bottom of the figure: maps of the P_{max} index corresponding to the same regions.

Table Captions

Table 1. Comparison between the resistivity of different kind of graphitic materials, created in different location (superficial or buried), and with different laser sources.